Higgsino dark matter in pure gravity mediated supersymmetry

Jason L. Evans[1] and Keith A. Olive[2]

[1]*Tsung-Dao Lee Institute, Shanghai Jiao Tong University, Shanghai 200240, China*
[2]*William I. Fine Theoretical Physics Institute, School of Physics and Astronomy, University of Minnesota, Minneapolis, Minnesota 55455, USA*

(Received 2 March 2022; accepted 24 June 2022; published 21 September 2022)

We consider the prospects for the direct detection of dark matter in pure gravity meditation (PGM) models of supersymmetry breaking. Minimal PGM models require only two parameters, the gravitino mass, $m_{3/2}$, which sets the UV mass for all scalar masses, and $\tan\beta$. Gaugino masses are generated through anomaly mediation. Typically the lightest supersymmetric state (the dark matter candidate) is a wino. Here, we consider a one-parameter extension of the minimal model by allowing the Higgs soft masses to deviate from universality. For simplicity, we take these to be equal and use the μ term as a surrogate. We also consider nonuniversal stop masses. When $|\mu| \sim 1$ TeV, the Higgsino is a viable dark matter candidate when the gravitino mass is of order $\sim$1 PeV and $\tan\beta \simeq 2$. We calculate the spin-dependent and spin-independent cross sections for dark matter scattering on protons. For spin-independent scattering, existing experimental limits place constraints on the PGM parameter space. Much of the currently allowed parameter space lies above the irreducible neutrino background. Thus, future direct detection experiments will be able to probe much of the remaining PGM parameter space.

DOI: 10.1103/PhysRevD.106.055026

I. INTRODUCTION

One of the appeals of supersymmetric theories is that they are capable of connecting multiple puzzles of nature within a single framework. For example, supersymmetry explains the radiative stability of the Higgs boson mass [1], has a dark matter candidate [2,3], provides for a stable electroweak vacuum [4], is consistent with a 125 GeV Higgs bosons mass [5], and leads to rather precise gauge coupling unification and so can explain charge quantization [6]. No other model has achieved such a high level of correlation between beyond the standard model puzzles. It truly is a paradigm worthy of our attention.

However, current constraints coming from the LHC put the scale of supersymmetry breaking masses beyond the TeV mass [7]. Although this does reduce the protection of the Higgs mass from radiative correction, it does not force us to sacrifice the other successes of supersymmetry. In fact, if we accept some fine-tuning in the Higgs sector, some of the challenges of building a successful supersymmetric model can be alleviated, like the Polonyi problem [8,9]. This thinking has motivated the study of models like split supersymmetry [10] or pure gravity mediation (PGM) with a large gravitino mass [11–18]. In the latter, the only source of supersymmetry breaking in the minimal supersymmetric standard model (MSSM) is the gravitino mass, $m_{3/2}$. Sfermion masses are generated at tree level and so are of the order of the gravitino mass. The gaugino masses are generated at the one-loop level from anomaly mediation [19] and so are also proportional to $m_{3/2}$. Even with large sfermion masses in pure gravity mediation, the other salient features of supersymmetric models like a wimp dark matter candidate are preserved since the gauginos are relatively light.

PGM models can be viewed among the most minimal set of supersymmetric models with radiative electroweak symmetry breaking (EWSB) [20] and full sfermion mass universality [14]. In the context of minimal supergravity, in addition to the gaugino masses, supersymmetry breaking trilinear terms, A_0, are also set by anomaly mediated interactions and are also proportional to the gravitino mass. Supergravity conditions then fix the Higgs bilinear supersymmetry breaking term, $B_0 = A_0 - m_{3/2} \simeq -m_{3/2}$ [21,22]. Minimization of the Higgs potential then fixes the μ term and the ratio of Higgs vacuum expectation values, $\tan\beta$. This single parameter model is however overconstrained, but can be relaxed by adding a Giudice-Masiero (GM) term [23–25] to the Kähler potential. In practice, one can then trade the GM term for $\tan\beta$ and use the EWSB conditions to determine the GM coupling. This leaves two free parameters, $m_{3/2}$ and $\tan\beta$.

The typical and most widely studied dark matter candidate in pure gravity mediated models is the wino. Because of the anomaly mediated gaugino mass conditions, the wino tends to be the lightest supersymmetric particle (LSP). Its relic density, determined by annihilations, is relatively insensitive to the sfermion mass spectrum, and a wino of mass of order 3 TeV can lead to the correct relic density [26–28] after inclusion of Sommerfeld enhancement effects [29]. Furthermore, if the wino is the dark matter candidate and produced from thermal freeze-out, there is a clear prediction for the sfermion mass spectrum. Indeed, the correct relic density ($\Omega h^2 \approx 0.12$ [30]) is obtained in PGM models when $m_{3/2} \sim 800$ TeV [17], making the prospects for the detection of sfermions at the LHC practically nonexistent. Instead, we expect relatively strong signals from indirect dark matter experiments. In fact, there is currently some tension with the H.E.S.S. experiment unless the galaxy dark matter profile is of the most cored variety [31–33]. This has led to concerns about the viability of wino dark matter.

Although these arguments do not decisively rule out wino dark matter, the exploration of other dark matter candidates in models like pure gravity mediation are warranted [17]. For example, by including additional vectorlike multiplets [16], it is possible that either the bino or gluino becomes the LSP. In this work, we revisit the simpler possibility of Higgsino dark matter in pure gravity mediation [17]. The Higgsino becomes the LSP when $\mu \ll m_{\tilde{W}}$. This can be achieved if one [34] or both [35] of the Higgs soft masses is nonuniversal and differ from $m_{3/2}$ [15]. Higgsino dark matter in related models has been discussed in [36–41]. Here, we specifically concentrate on the prospects of the direct detection of dark matter in PGM models.

As we will show, the prospect for the direct detection of a Higgsino dark matter candidate in PGM models is quite good. This is due to the fact that gauginos are necessarily loop-suppressed relatively to the sfermion masses, most importantly the stop masses. The upper bound on the Higgs boson mass then places an upper bound on the gauginos masses. This then necessarily leads to a nontrivial mixing angle between the bino, wino, and Higgsinos. Since LSP-nucleon scattering comes at the cost of a single Higgsino-bino or Higgsino-wino mixing angle, the cross section can be large enough to be measured in direct detection experiments for most if not all of the parameter space. In fact, a majority of the parameter space of Higgsino dark matter in PGM will be probed by the upcoming direct detection experiments. In contrast, other split supersymmetry models, which do not require the gaugino mass suppression relative the sfermion masses to be at the one-loop level, will have large regions of parameter space inaccessible to direct detection experiments.

In what follows, we briefly review the basic idea behind pure gravity mediation in Sec. II. While the minimal model can be described by two parameters, $m_{3/2}$ and $\tan\beta$, the models considered here contain a third parameter, μ which is equivalent to nonuniversal Higgs masses. Furthermore, we also consider the effect of allowing the stop mass to be nonuniversal. As in earlier work [17], we find a viable Higgsino-like dark matter candidate with acceptable Higgs masses when $m_{3/2} \sim 1$ PeV, $\tan\beta \sim 2$, and $|\mu| \sim 1$ TeV. In Sec. III, we describe our calculation of the scattering cross sections. Our results are presented in Sec. IV and our conclusions are given in Sec. V.

II. PURE GRAVITY MEDIATION

In this section, we discuss a few details of minimal pure gravity mediation and its realization with nonuniversal soft masses. For more details see [15,17].

The core idea of pure gravity mediation is that all supersymmetry breaking in the visible sector comes from gravity. In this scenario, the soft masses are generated the same way they are in minimal supergravity (mSUGRA), i.e., with a flat Kähler potential, by a correction to the scalar potential coming from Planck suppressed operators, and are of order $m_{3/2}$. In mSUGRA, we expect scalar mass universality at the scale supergravity is broken. This avoids problems with flavor changing neutral currents [42]. In PGM, we take universal scalar masses only for simplicity, since as we will see, the large values needed for $m_{3/2}$ preclude the problems with flavor changing neutral currents. Since these masses are proportional to the expectation value of the superpotential, they do not *a priori* depend explicitly on any singlets. The gaugino masses, on the other hand, for models like mSUGRA, do generally depend on a singlet (through a nontrivial gauge kinetic function). In order to get a gaugino mass of order $m_{3/2}$ from gravitational interactions, a singlet supersymmetry breaking field which couples to the gauge fields of the following form is needed:

$$W \supset \frac{cZ}{M_P}\mathcal{W}\mathcal{W}. \tag{1}$$

If the field is not a singlet, this term is forbidden and the leading order contribution is of higher order and thus very suppressed.

With the gravity mediated contribution to the gauginos masses suppressed, the anomaly mediated contribution [19] becomes dominant. In this case, gaugino masses take the form

$$M_1 = \frac{33}{5}\frac{g_1^2}{16\pi^2}m_{3/2}, \tag{2}$$

$$M_2 = \frac{g_2^2}{16\pi^2}m_{3/2}, \tag{3}$$

$$M_3 = -3\frac{g_3^2}{16\pi^2}m_{3/2}, \tag{4}$$

where g_i are the electroweak and strong gauge couplings and we see that the gaugino masses are loop suppressed compared to sfermion masses. Note that contributions from Higgsino loops can be neglected if $\mu \ll m_{3/2}$.

As noted above, in the minimal setup of PGM, the Kähler potential is taken to be flat. Scalar masses are universal and equal to gravitino mass at some high energy input scale which we take here to be the scale of gauge coupling unification. Gaugino masses and supersymmetry breaking trilinear A terms are loop suppressed. Additionally, from what we know in mSUGRA, the B term is fixed at the input scale to be $B_0 = A_0 - m_{3/2} \approx -m_{3/2}$. Thus the only free parameters are $m_{3/2}$, $\tan\beta$, and μ. However, the minimization of the Higgs potential then fixes two of these, leaving a single parameter theory which is overly restrictive. If a GM term is included in the Kähler potential,

$$\Delta K = c_H H_1 H_2 + \text{H.c.}, \tag{5}$$

where c_H is a constant, the expressions for μ and B are modified at the input scale,

$$\mu = \mu_0 + c_H m_{3/2}, \tag{6}$$

$$B\mu = \mu_0(A_0 - m_{3/2}) + 2c_H m_{3/2}^2. \tag{7}$$

As a result, after minimization of the Higgs potential, there are two remaining free parameters[1] which can be chosen to be $\tan\beta$ and $m_{3/2}$ (so that μ and c_H are determined by EWSB). Generically, this minimal model has a wino dark matter candidate[2] with the correct thermal relic density for a gravitino mass of order 800 TeV.

In this work, we examine a slightly more generic scenario with nonuniversal Higgs masses [15,17]. This can be accomplished by the addition of higher dimensional operators involving the supersymmetry breaking field and the Higgs fields. We take the following Kähler potential,

$$K = yy^* + K^{(H)} + K^{(Z)} + \log|W|^2, \tag{8}$$

where

$$K^{(Z)} = ZZ^*\left(1 - \frac{ZZ^*}{\Lambda^2}\right), \tag{9}$$

and

$$K^{(H)} = \left(1 + a\frac{ZZ^*}{M_P^2}\right)H_1H_1^* + \left(1 + b\frac{ZZ^*}{M_P^2}\right)H_2H_2^* + (c_H H_1 H_2 + \text{H.c.}), \tag{10}$$

and y represents all other MSSM fields other than the Higgs bosons, H_1, H_2, W is the MSSM superpotential, and Z is the supersymmetry breaking field which we assume is strongly stabilized at some mass scale $\Lambda < M_P$ [9,44,45]. We do not contemplate the origin of these higher dimensional operators and consider this only as an effective theory. For this Kähler potential, all MSSM sfermion fields get soft masses equal to $m_{3/2}$ with the exception of the Higgs soft masses. If Z is a Polonyi-like field, its expectation value induces an F term and both the Higgs soft masses become free parameters given by the constants a and b. The two soft Higgs masses are $m_{H_1}^2 = (1-3a)m_{3/2}^2$ and $m_{H_2}^2 = (1-3b)m_{3/2}^2$.

Our ability to obtain a Higgsino dark matter candidate is simplified if we allow μ to be a free input parameter. Thus we require only one additional input parameter and we take $m_{H_1}^2 = m_{H_2}^2$ or $a = b$. Typically, the Higgs masses are set at the grand unified theory (GUT) scale and then are renormalization group evolved to the weak scale. The Higgs potential minimization conditions are then used to determine μ and in this case c_H (since B_0 is fixed in mSUGRA and we keep $\tan\beta$ free). We will instead use μ as an input and use the Higgs potential minimization conditions to determine $m_{H_2}^2$ and c_H and $m_{H_1}^2$ is set equal to $m_{H_2}^2$ at the GUT scale. This implementation of nonuniversal Higgs masses has the advantage of being able to readily realize a Higgsino mass which gives the correct thermal relic density.

The range of mass scales considered in PGM models is large. Typical scalar masses are of order 1 PeV. Since we expect the Higgs scalar masses to be of the same order (if not equal), there are large cancellations which occur in the minimization of the Higgs potential which is used to determine μ. The μ term at the minimum is given by

$$\mu^2 = \frac{m_1^2 - m_2^2\tan^2\beta + \frac{1}{2}m_Z^2(1-\tan^2\beta) + \Delta_\mu^{(1)}}{\tan^2\beta - 1 + \Delta_\mu^{(2)}}, \tag{11}$$

where the correction terms are given by [46]

$$\begin{aligned}\Delta_\mu^{(1)} \approx & -\frac{3h_t^2}{16\pi}(f(m_{\tilde{t}_1}, m_Z) + f(m_{\tilde{t}_2}, m_Z) - 2f(m_t, m_Z))\tan^2\beta \\ & + \frac{3h_b^2}{16\pi}(f(m_{\tilde{b}_1}, m_Z) + f(m_{\tilde{b}_2}, m_Z) - 2f(m_b, m_Z)) \\ & + \frac{3h_\tau^2}{16\pi}(f(m_{\tilde{\tau}_1}, m_Z) + f(m_{\tilde{\tau}_2}, m_Z) - 2f(m_\tau, m_Z)),\end{aligned} \tag{12}$$

[1] See [14] for more details.

[2] Even in this minimal setup, a Higgsino dark matter candidate can be realized in a focus pointlike scenario [43]. However, as the fully universal mSUGRA-PGM model is a special case of our consideration here, it is included in our analysis.

and

$$\Delta_\mu^{(2)} \approx -\frac{3h_t^2}{16\pi}\frac{(f(m_{\tilde{t}_1},m_Z)+f(m_{\tilde{t}_2},m_Z))}{\tilde{t}_1^2-\tilde{t}_2^2} + \frac{3h_b^2}{16\pi}\frac{(f(m_{\tilde{b}_1},m_Z)+f(m_{\tilde{b}_2},m_Z))}{\tilde{b}_1^2-\tilde{b}_2^2} + \frac{3h_\tau^2}{16\pi}\frac{(f(m_{\tilde{\tau}_1},m_Z)+f(m_{\tilde{\tau}_2},m_Z))}{\tilde{\tau}_1^2-\tilde{\tau}_2^2}, \quad (13)$$

with

$$f(x,y) = x^2\left(\ln\left(\frac{x}{y}\right)-1\right). \quad (14)$$

In these expressions, we have ignored the contributions from A terms (which are very small in PGM models), though they are kept in our numerical evaluations. To have an idea of the scales involved, we choose a representative point with $m_0 = 1$ PeV, $\tan\beta = 1.8$ and $\mu = 1080$ GeV (the choice of this point will be clear shortly). In the Table, we list the relevant mass scales and corrections which determine μ as well as some of the weak scale spectrum. As one can see, the radiative corrections for the third generation can be quite substantial in the cancellations needed to obtain a TeV scale μ parameter.

To better understand the running of the various supersymmetry breaking parameters, we show in Fig. 1 (left) the running of the soft scalar masses from the GUT scale to the weak scale. All sfermion masses are equal to $m_{3/2} = 1$ PeV at the GUT scale. The two soft Higgs masses are set at 1.24 PeV. This value is fixed by the electroweak symmetry breaking conditions in order to obtain $\mu = 1080$ GeV. At low renormalization scale, Q, the running is terminated when $Q^2 = m^2(Q)$. Note that the electroweak symmetry is broken despite the fact that both soft Higgs masses remain positive. This is due to the large B term (or more precisely large $B\mu$ term) which at the tree level is the off-diagonal element in the Higgs mass^2 matrix. The value of B is given in the Table, but can also be determined from Eqs. (6) and (7). Indeed for this value of B (which like μ runs very little), the determinant of the mass^2 matrix turns negative as m_{H_2} runs to lower values. The running of the gaugino masses is shown in the right panel of Fig. 1.

Later we will consider a slightly more generic model where the stop soft masses are equal but different from the Higgs soft masses and other sfermion masses. This can be accomplished in the effective theory in a similar manner as was done in Eq. (10) for the Higgs masses. The purpose of considering nonuniversal stop masses is to attempt to capture the features of more generic models of pure gravity mediation beyond the minimal model. In pure gravity mediation models, because the soft masses are so large, order 1 changes in the soft masses have minimal effect on the low-scale theory except for the stop masses and Higgs masses. The Higgs boson masses play an important role in radiative electroweak symmetry breaking and in determining the mass of the Higgsino. The stop masses, on the other hand, play an important role in determining the standard model Higgs boson mass. By taking the Higgs and stop soft masses nonuniversal, we are able to capture the major features of a more generic pure gravity mediation model and see how Higgsino dark matter would look in this scenario. Thus, for this work we take a model with the following set of free parameters:

$$m_{3/2}, \qquad \tan\beta, \qquad \mu, \qquad m_T, \quad (15)$$

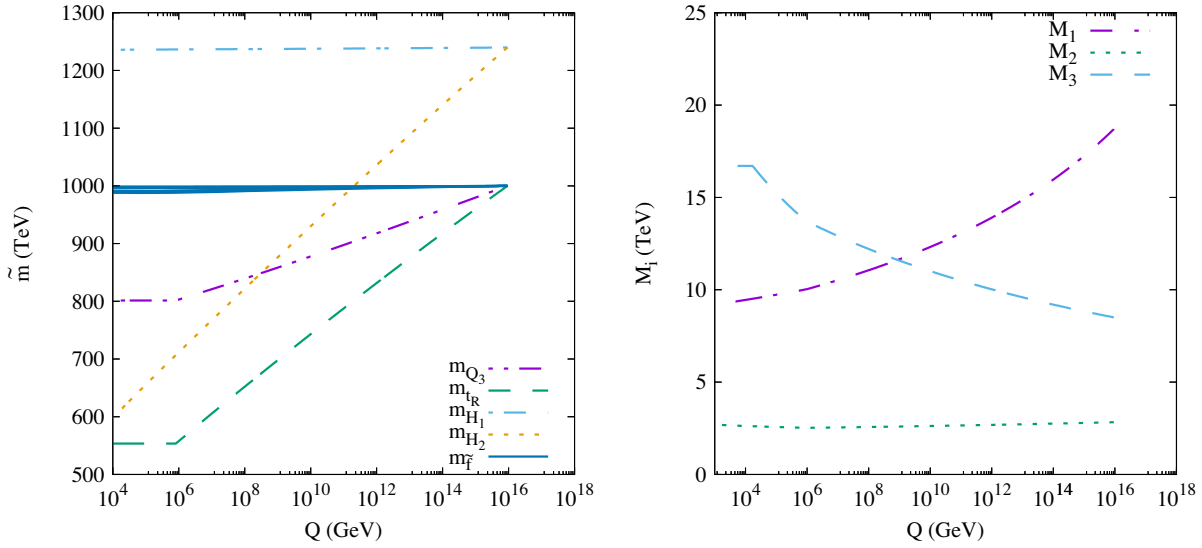

FIG. 1. The running of the soft scalar masses from the GUT scale to the weak scale. Left: all sfermion masses are input at 1 PeV, while the soft Higgs masses are set at 1.24 PeV. The lines labeled by $m_{\tilde{f}}$ which are narrowly split are for $m_{\tilde{b}_R}$, $m_{\tilde{L}_3}$, $m_{\tilde{\tau}_R}$, $m_{\tilde{Q}_1}$, $m_{\tilde{u}_R}$, $m_{\tilde{d}_R}$, $m_{\tilde{L}_1}$, and $m_{\tilde{e}}$. Right: the gaguino masses are input with their anomaly mediated value for $m_{3/2} = 1$ Pev.

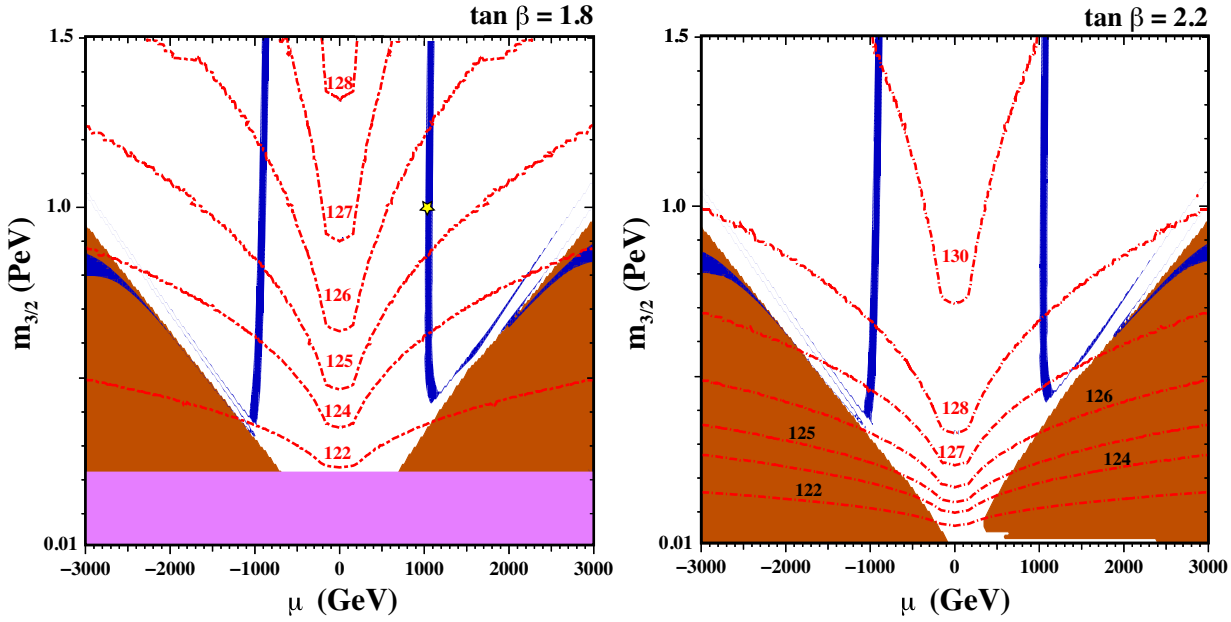

FIG. 2. The $(\mu, m_{3/2})$ plane for fixed $\tan\beta = 1.8$ (left) and 2.2 (right). The pink shaded region is excluded as it contains a tachyonic stop. In the dark red shaded region, there is a wino LSP. In the remainder of the plane, the Higgsino is the LSP. Higgs mass contours, with masses labeled are shown as red dot-dashed curves. In the dark blue strips, the relic density is $\Omega_\chi h^2 = 0.11$–0.13. The yellow star corresponds to the point in Table I.

where the gravitino mass is the mass of all the scalar particles at GUT scale except the stops and the Higgs bosons, and m_T is the mass of left- and right-handed stop masses at the input scale (thus also equal to $m_{\tilde{b}_L}$, while $m_{\tilde{b}_R} = m_{3/2}$). Initially, we will take $m_T = m_{3/2}$ and then later consider this full set of parameters.

TABLE I. Parameters and predictions of a PGM point that yields values of $\Omega_\chi h^2$ and m_h that are consistent with experiment. This point corresponds to the star in the left panel of Fig. 2.

Higgs mass parameters (masses in PeV units)		
$m_{H_1} = 1.23$	$m_{H_2} = 0.47$	$\mu = 0.0011$
$B = 780$	$\sqrt{\Delta_\mu^1} = 0.90$	$\Delta_\mu^2 = -0.28$
Input supersymmetry parameters (masses in TeV units)		
$m_{3/2} = 1000$	$\tan\beta = 1.8$	$c_H = -0.30$
$a = -0.18$	$b = -0.18$	
MSSM particle masses (in PeV units)		
$m_\chi = 0.0011$	$m_{\tilde{t}_1} = 0.55$	$m_{\tilde{g}} = 0.22$
$m_{\chi_2} = 0.0011$	$m_{\chi_3} = 0.0035$	$m_{\chi_4} = 0.010$
$m_{\tilde{t}_2} = 0.80$	$m_{\tilde{b}_1} = 0.80$	$m_{\tilde{b}_2} = 0.99$
$m_{\tilde{q}_L} = 0.99$	$m_{\tilde{d}_R} = 0.99$	$m_{\tilde{u}_R} = 0.99$
$m_{\tilde{\mu}_R} = 1.00$	$m_{\tilde{\mu}_L} = 1.00$	$m_{\tilde{\tau}_1} = 1.00$
$m_{\tilde{\tau}_2} = 1.00$	$m_{\chi_1^\pm} = 0.0011$	$m_{\chi_2^\pm} = 0.0035$
$m_{H,A} = 1.41$	$m_{H^\pm} = 1.41$	
Other observables		
$\Omega_\chi h^2 = 0.125$	$m_h = 125.4$ GeV	

The restricted parameter space (with $m_T = m_{3/2}$) was previously studied [17] and we present some updated results in the $(\mu, m_{3/2})$ planes shown in Fig. 2 for fixed values of $\tan\beta = 1.8$ and 2.2. For $\tan\beta = 1.8$ and $m_{3/2} \lesssim 200$ TeV, one of the stops is tachyonic and that excluded region is shaded pink. The dark red shaded regions contain a wino LSP. In the unshaded regions, there is a Higgsino LSP. The LSP mass contours are not shown but the wino LSP mass is determined primarily from anomaly mediation with $m_{\tilde{W}} \approx 0.27 m_{3/2}$. The mass of the Higgsino depends primarily on μ, $m_{\tilde{H}} \approx 1.1\mu$. For both states, there is a slight dependence on the sign of μ and $\tan\beta$. The values of the Higgs mass are shown by a series of red dot-dashed contours as labeled. As one can see, there is a strong dependence of the Higgs mass on $\tan\beta$. For $\tan\beta > 2.2$ and the large values of $m_{3/2}$ we considered, the Higgs mass begins to exceed the experimental value even if a relatively large theoretical uncertainty is assigned to the Higgs mass calculation. At $\tan\beta < 1.8$, renormalization group evolution inevitably leads to a tachyonic stop for small $m_{3/2}$ and is excluded.

In the dark blue shaded strips of Fig. 2, the LSP has a relic density $\Omega h^2 = 0.11$–0.13. Note that this range is taken to be significantly wide than the Planck results [30] which indicate a cold dark matter density of $\Omega_c h^2 = 0.1200 \pm 0.0012$ and enhances the visibility of these strips. The thermal relic density in the Higgsino region depends primarily on the mass of the Higgsino [36] and the desired abundance is achieved when $\mu \approx -900$ GeV and 1080 GeV, with a Higgsino mass just over 1100 GeV for both positive

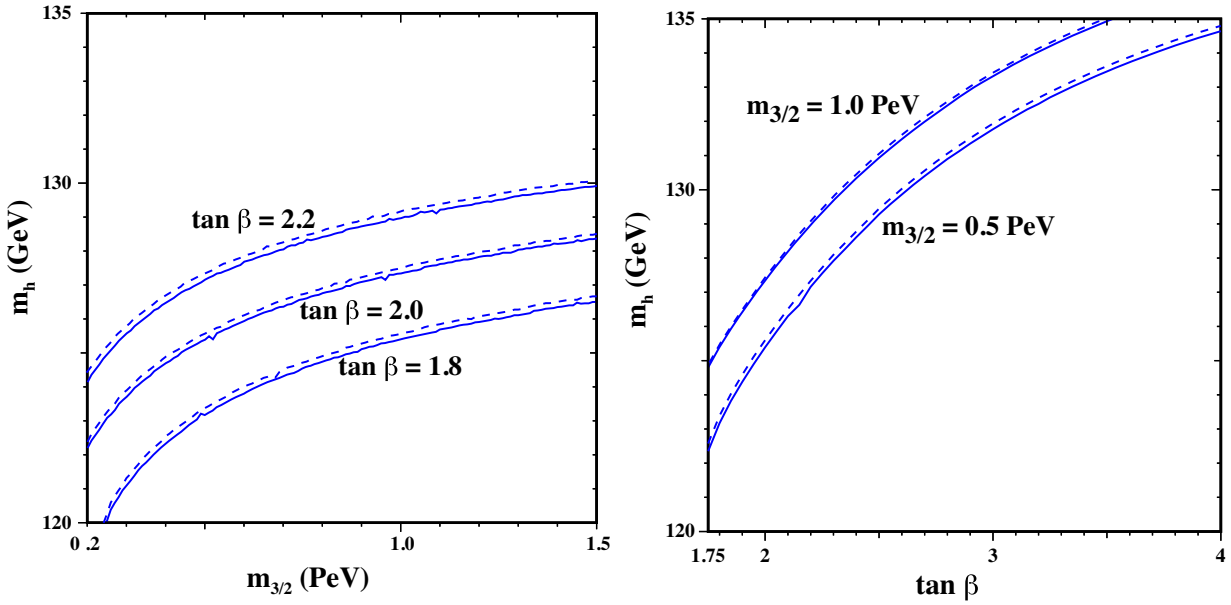

FIG. 3. Left: the Higgs mass vs $m_{3/2}$ for three values of $\tan\beta = 1.8$, 2.0, and 2.2. Right: the Higgs mass vs $\tan\beta$ for two values of $m_{3/2} = 0.5$ and 1.0 PeV. The value of μ is fixed to 1080 GeV (solid) and -900 GeV (dashed).

and negative μ (the sign dependence on μ in the Higgsino mass calculation is due to one-loop threshold corrections). The preferred regions are seen as the vertical strips in both panels. In the dark red shaded region at large $|\mu|$ and $m_{3/2} \approx 800$ TeV, the wino is the LSP and $\Omega h^2 \approx 0.12$. One also finds three very thin dark blue diagonal strips where the desired relic density can be obtained through coannihilations between the wino and two Higgsinos which are all nearly degenerate in that region. These have been discussed in more detail in [17]. Our primary interest here is the nearly vertical relic density strips.

We show the dependence of the Higgs mass on both the gravitino mass and $\tan\beta$ in Fig. 3. We plot m_h vs $m_{3/2}$ for three values of $\tan\beta = 1.8$, 2.0, and 2.2. The value of μ is fixed to 1080 GeV and shown as solid curves and -900 GeV as dashed curves. As one can see, this range of $\tan\beta$ covers the experimentally acceptable values of m_h for a wide range of gravitino masses. Note again that the stop mass becomes tachyonic for $\tan\beta \lesssim 1.8$. In the right panel we see the rapid increase in m_h with $\tan\beta$, for fixed values of $m_{3/2} = 0.5$ and 1 PeV.

As noted above, the models considered have nonuniversal Higgs masses, which are set equal to each other at the GUT scale. The degree of nonuniversality required is shown in Fig. 4 which shows the value of $a = \frac{1}{3}(1 - m_{H_1}^2/m_{3/2}^2)$ as a function of the gravitino mass (assuming $m_{H_1} = m_{H_2}$). For the displayed curves, $\mu = 1080$ GeV, and as a function of $m_{3/2}$ they track the right blue shaded region in each panel of Fig. 2. The curves for the left blue shaded regions (with $\mu = -900$ GeV) would be nearly identical. As one can see, for $\tan\beta = 1.8$, universality is only achieved for very large $m_{3/2}$ where the Higgs mass is significantly larger than 125 GeV. However, for $\tan\beta = 2.2$ complete scalar mass universality is achieved when $m_{3/2} = 0.49$ PeV, and the Higgs mass is 127.1 GeV. We also show the corresponding curve with $\tan\beta = 2.0$. In this case, universality occurs at $m_{3/2} = 1.35$ PeV, but there $m_h = 128.1$ GeV.

III. DIRECT DETECTION OF HIGGSINO DARK MATTER

It is straightforward to calculate the elastic scattering cross section for a neutralino on a nucleon [47–49]. Here we simply quote the most important ingredients from [49] for the purpose of studying Higgsino elastic scattering. We consider only spin-dependent and spin-independent interaction from the four-fermi Lagrangian for χ-nucleon scattering:

$$\mathcal{L} \ni \alpha_{2i}\bar{\chi}\gamma^\mu\gamma^5\chi\overline{q_i}\gamma_\mu\gamma^5 q_i + \alpha_{3i}\bar{\chi}\chi\overline{q_i}q_i. \tag{16}$$

If we ignore the contributions from squark exchange as well as the heavy Higgs scalar exchange,[3] the coefficients α_i can be written as

$$\alpha_{2i} \simeq -\frac{g^2}{4m_Z^2\cos^2\theta_W}[|Z_{\chi_3}|^2 - |Z_{\chi_4}|^2]\frac{T_{3i}}{2}, \tag{17}$$

and

[3]Though these contributions are negligible for the cases under study, they are included in all our numerical work.

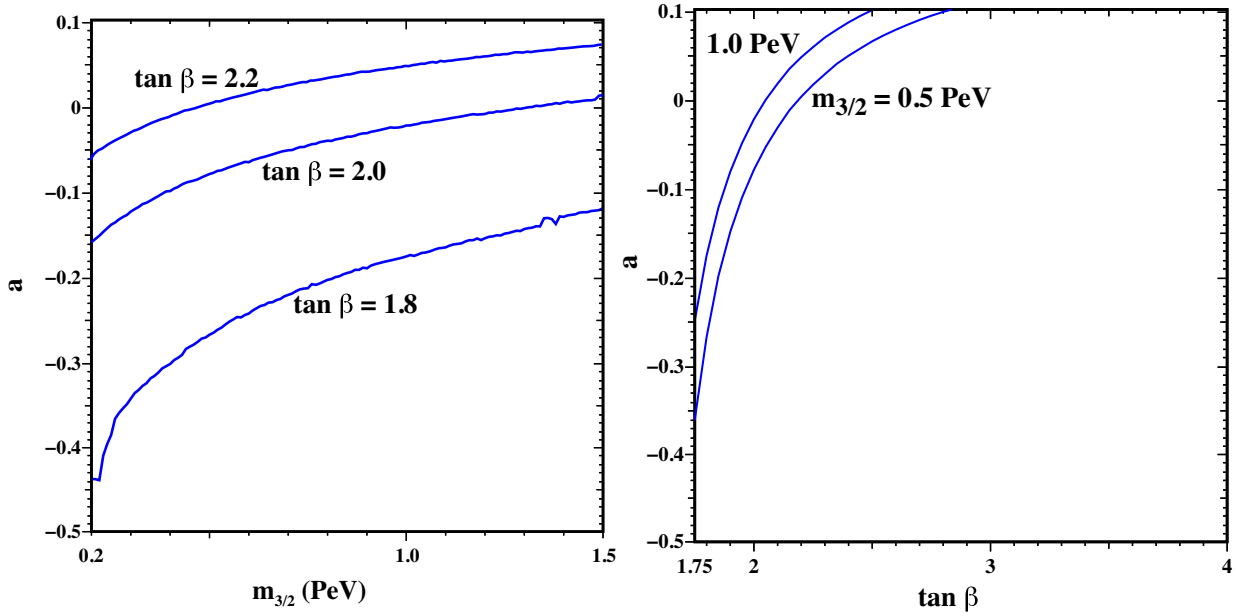

FIG. 4. Left: the degree Higgs mass nonuniversality for three values of $\tan\beta = 1.8$, 2.0, and 2.2. Plotted is the Kähler coupling $a = \frac{1}{3}(1 - m_{H_1}^2/m_{3/2}^2)$ vs $m_{3/2}$. Full scalar mass universality corresponds to $a = 0$. Right: Kähler coupling a vs $\tan\beta$ for two values of $m_{3/2} = 0.5$ and 1.0 PeV. This plot assumes $\mu = 1080$ GeV, but would be nearly identical for $\mu = -900$ GeV.

$$\alpha_{3i} \simeq -\frac{g m_{qi}}{4 m_W m_h^2 B_i}[\mathrm{Re}(\delta_{1i}[gZ_{\chi 2} - g' Z_{\chi 1}])D_i C_i + \mathrm{Re}(\delta_{2i}[gZ_{\chi 2} - g' Z_{\chi 1}])D_i^2,], \tag{18}$$

where T_{3i} denotes isospin for up type ($i = 1$) and down type ($i = 2$) quarks, and $Z_{\chi j}$ corresponds to the $\tilde{B}, \tilde{W}, \tilde{H}_1, \tilde{H}_2$ component of the LSP for $j = 1, 2, 3, 4$ respectively, and

$$\delta_{1i} = Z_{\chi 3}(Z_{\chi 4}), \qquad \delta_{2i} = Z_{\chi 4}(-Z_{\chi 3}), \tag{19}$$

$$B_i = \sin\beta(\cos\beta), \quad C_i = \sin\alpha(\cos\alpha), \quad D_i = \cos\alpha(-\sin\alpha), \tag{20}$$

for up (down) type quarks. We denote by m_h the mass of the light scalar Higgs and α denotes the Higgs mixing angle.

The mixing angles of a Higgsino LSP with the different neutralino components can be approximated as

$$Z_{\chi 1} = -\frac{\sqrt{2}}{2}(c_\beta \pm s_\beta)\frac{M_Z s_W}{M_1 - |\mu|} + \mathcal{O}(M_Z^3), \tag{21}$$

$$Z_{\chi 2} = \frac{\sqrt{2}}{2}(c_\beta \pm s_\beta)\frac{M_Z c_W}{M_2 - |\mu|} + \mathcal{O}(M_Z^3), \tag{22}$$

$$Z_{\chi_3} = \mp\frac{\sqrt{2}}{2} \pm \frac{\sqrt{2}}{8}\left(\frac{c_W^2(c_\beta^2 - s_\beta^2)}{|\mu|(M_2 - |\mu|)} + \frac{c_W^2(c_\beta \pm s_\beta)^2}{(M_2 - |\mu|)^2} + \frac{s_W^2(c_\beta^2 - s_\beta^2)}{|\mu|(M_1 - |\mu|)} + \frac{s_W^2(c_\beta \pm s_\beta)^2}{(M_1 - |\mu|)^2}\right)M_Z^2 + \mathcal{O}(M_Z^3), \tag{23}$$

$$Z_{\chi_4} = \frac{\sqrt{2}}{2} + \frac{\sqrt{2}}{8}\left(\frac{c_W^2(c_\beta^2 - s_\beta^2)}{|\mu|(M_2 - \mu)} - \frac{c_W^2(c_\beta \pm s_\beta)^2}{(M_2 - \mu)^2} + \frac{s_W^2(c_\beta^2 - s_\beta^2)}{|\mu|(M_1 - \mu)} - \frac{s_W^2(c_\beta \pm s_\beta)^2}{(M_1 - \mu)^2}\right)M_Z^2 + \mathcal{O}(M_Z^3), \tag{24}$$

where $s_\beta = \sin\beta$, $c_\beta = \cos\beta$, $c_W = \cos\theta_W$, and $s_W = \sin\theta_W$ and the upper (lower) sign is for $\mu > 0$ ($\mu < 0$). This approximation is valid as long as the LSP is predominantly Higgsino and $M_Z/(M_2 - |\mu|) \ll 1$. Using these approximate relations and taking the decoupling limit where $\alpha = \beta - \frac{\pi}{2}$, α_{3i} and α_{2i} can be simplified to

$$\alpha_{2i} \simeq -\frac{1}{8}\cos^2\beta(1 - \tan^2\beta) \times \left(\frac{g'^2}{|\mu|(M_1 - |\mu|)} + \frac{g^2}{|\mu|(M_2 - |\mu|)}\right)\frac{T_{3i}}{2}, \tag{25}$$

and

$$\alpha_{3i} \simeq -\frac{1}{8}\frac{m_{q_i}\cos^2\beta(1 \pm \tan\beta)^2}{m_{H_2}^2}\left(\frac{g'^2}{M_1 - |\mu|} + \frac{g^2}{M_2 - |\mu|}\right). \tag{26}$$

We have checked that numerically these expressions are quite accurate for much of the parameter space we consider. In fact, even for $M_2 - |\mu| \sim 400$ GeV, these expressions are still accurate to within about 5%.

The spin-independent scattering cross section for the LSP on a proton can be written as

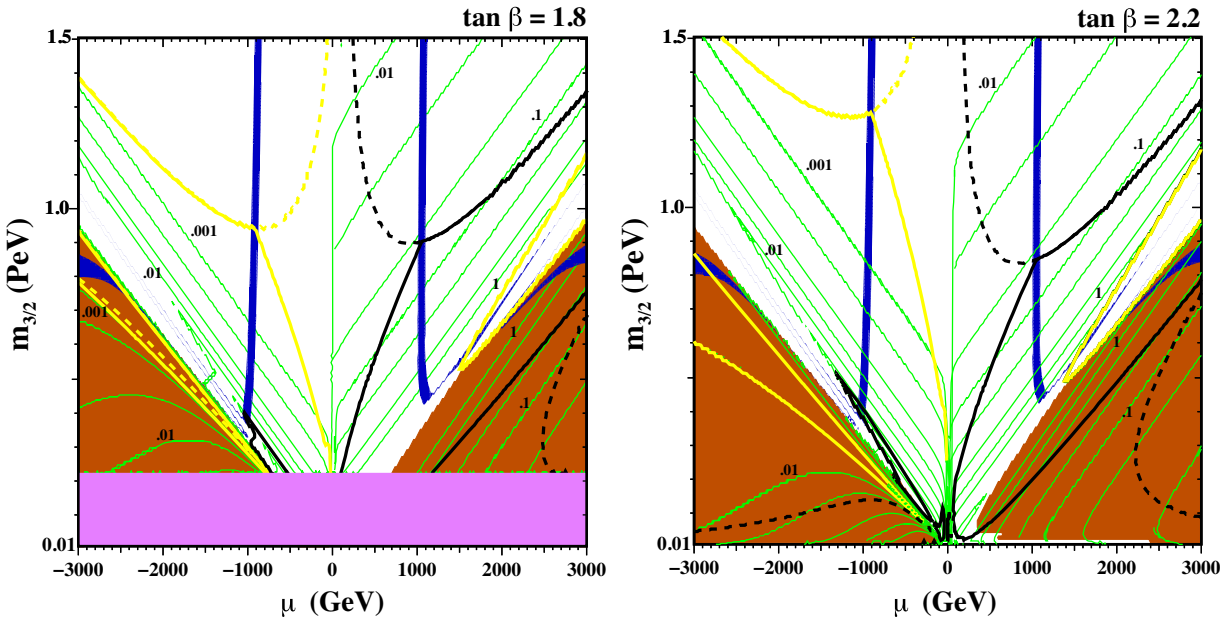

FIG. 5. The spin-independent elastic cross section for LSP scattering on protons in the $(\mu, m_{3/2})$ plane for fixed $\tan\beta = 1.8$ (left) and 2.2 (right). The shaded regions are the same as in Fig. 2. Values of the cross sections are as labeled in units of 10^{-8} pb. Contours between the labeled decades are 2× and 5× the preceding decade. Also shown as thick black curves are contours for the current experimental bound from PandaX-4T [52]. Solid contours correspond to the scaled limit when the relic density is < 0.12. The neutrino floor is shown by the thick yellow contour.

$$\sigma_3 = \frac{4m_r^2}{\pi} f_p^2, \tag{27}$$

where m_r is the reduced LSP mass, and

$$\frac{f_p}{m_p} = \sum_q f_{Tq}^{(p)} \frac{\alpha_{3q}}{m_q}. \tag{28}$$

The parameters $f_{Tq}^{(p)}$ are defined by

$$m_p f_{Tq}^{(p)} \equiv \langle p|m_q \bar{q} q|p\rangle, \tag{29}$$

and have recently been reevaluated [50]:

$$\begin{aligned} f_{Tu}^{(p)} &= 0.018 \pm 0.005, & f_{Td}^{(p)} &= 0.027 \pm 0.007, & f_{Ts}^{(p)} &= 0.037 \pm 0.017 \\ f_{Tc}^{(p)} &= 0.078 \pm 0.002, & f_{Tb}^{(p)} &= 0.072 \pm 0.002, & f_{Tt}^{(p)} &= 0.069 \pm 0.001. \end{aligned} \tag{30}$$

The spin-dependent elastic χ-proton cross section can be written as

$$\sigma_2 = \frac{24}{\pi} G_F^2 m_r^2 a_p^2, \tag{31}$$

where

$$a_p = \sum_i \frac{\alpha_{2i}}{\sqrt{2} G_f} \Delta_i^{(p)}. \tag{32}$$

The factors $\Delta_i^{(p,n)}$ parametrize the quark spin content of the nucleon [50],

$$\begin{aligned} \Delta_u^{(p)} &= 0.84 \pm 0.03, & \Delta_d^{(p)} &= -0.43 \pm 0.03, \\ \Delta_s^{(p)} &= -0.09 \pm 0.03. \end{aligned} \tag{33}$$

IV. RESULTS

Despite the very large scalar masses associated with PGM models, the Higgsino as a dark matter candidate still lends itself to the possibility of detection in direct detection experiments. As we will see, although some of the parameter space described above is already excluded by existing data, a substantial range in parameters remains viable and potentially detectable in future experiments, as much of the parameter space predicts scattering cross sections in excess of the so-called neutrino floor [51].

In Fig. 5, we show the same $(\mu, m_{3/2})$ planes as in Fig. 2 with $\tan\beta = 1.8$ (2.2) in the left (right) panels, and provide contours of the spin-independent cross sections, $\sigma_p^{\rm SI} = \sigma_3$. Contour labels correspond to units of 10^{-8} pb. Unlabeled contours correspond to 2× and 5× within each decade.

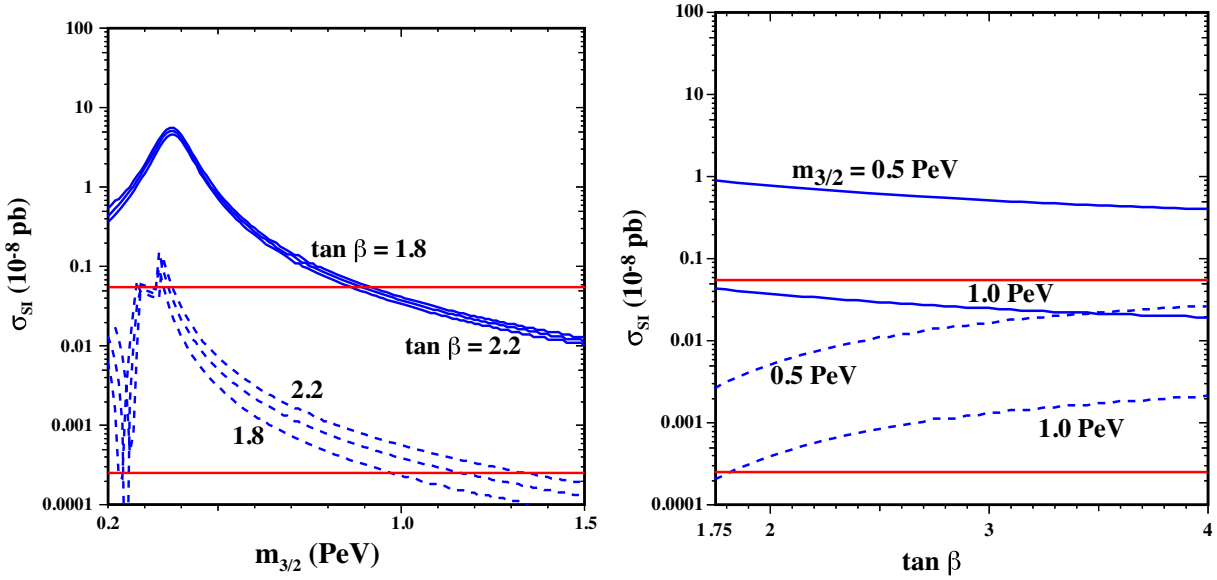

FIG. 6. The spin-independent elastic cross section for LSP scattering on protons as a function of $m_{3/2}$ (left) for $\tan\beta = 1.8$, 2.0, and 2.2, and as a function of $\tan\beta$ (right) for $m_{3/2} = 0.5$ and 1.0 PeV. In both panels, $\mu = 1080$ GeV (solid) and -900 GeV (dashed). The upper and lower horizontal lines in the left panels correspond to the limit from PandaX-4T [52] and the neutrino floor respectively.

We also show the current bound from the PandaX-4T commissioning run [52] as black contours. In the Higgsino region (unshaded), the allowed parameter space is above the black line, while in the wino region (shaded), it is below the line. These bounds are relevant only for $\mu > 0$ as there are significant cancellations for $\mu < 0$ which suppress the cross section [49,53–55], sometimes known as blind spots. This cancellation can be understood from examining Eq. (26). Since we consider $\tan\beta$ close to 1, α_{3i} is strongly suppressed for $\mu < 0$ as compared to $\mu > 0$, as can be see in Eq. (26). For $\mu \gtrsim 1.1$ TeV, (i.e., to the right of the nearly vertical blue strip), the relic Higgsino density from thermal freeze-out exceeds the observed cold dark density and is only viable if there is an additional (post freeze-out) source of entropy production. In this regime, the bound on the cross section (at roughly 10^{-9} pb) weakens slightly as the Higgsino mass (μ) increases. At lower μ, the thermal relic density is too low and we have scaled the cross section bound by $\Omega_\chi h^2/0.12$ to reflect the lower density (and hence scattering rates). In the event that there is a nonthermal source of Higgsinos, the unscaled limit is shown as a dashed black curve which strengthens significantly as the mass is lowered (either lower μ, or lower $m_{3/2}$ in the wino region).

Although there is currently no significant experimental constraint on the parameter space when $\mu < 0$ [except for the small loop around $(-1, 300)$ TeV], much of the parameter space is potentially detectable in future experiments. The yellow contours in Fig. 5 show the position of the neutrino floor [51] below which direct detection becomes overwhelmed by the inevitable neutrino background. For $\mu > 0$, the cross section drops below the neutrino floor only in the wedge near the Higgsino/wino boundary. There is actually a black contour below the yellow as the cross section drops precipitously when the LSP changes from an antisymmetric Higgsino ($[\tilde{H}_1 - \tilde{H}_2]/\sqrt{2}$) to a symmetric combination ($[\tilde{H}_1 + \tilde{H}_2]/\sqrt{2}$) [36] causing a strong cancellation. A similar wedge (without a black contour) is seen when $\mu < 0$ when the LSP changes from a Higgsino to a predominantly wino. The dashed contour again ignores the fact that the relic density is low and does not include a scaling of the cross section. For $\mu < 0$, outside the wedge, only the portion of the plane above the yellow contour is potentially unobservable.

Some of this behavior is more easily understood in the one-dimensional plots shown in Fig. 6. In the left panel, we show the spin-independent cross section as a function of the gravitino mass, while in the right panel as a function of $\tan\beta$. We have chosen values of μ so that we obtain the correct thermal relic density in the Higgsino region, $\mu = 1080$ GeV (solid curves) and $\mu = -900$ (dashed curves). Consider for example the spin-independent cross section $\mu > 0$. For low $m_{3/2}$, the wino is the LSP, and the cross section rises with $m_{3/2}$ to a maximum, and then drops once the LSP becomes Higgsino-like. There is little $\tan\beta$ dependence, which is also seen in the right panel where the curves (for fixed $m_{3/2}$) are rather flat. In both panels, the upper horizontal red line represents the current 90% upper limit from PandaX-4T [52] for a ∼1 TeV LSP. This limit excluded values of $m_{3/2} \lesssim 850$ TeV for $\mu > 0$. The lower horizontal red line corresponds to the neutrino floor for a ∼1 TeV LSP. All of the predicted cross sections shown lie above the floor and are in principle detectable. For $\mu < 0$, there are significant cancellations which occur in Eq. (18)

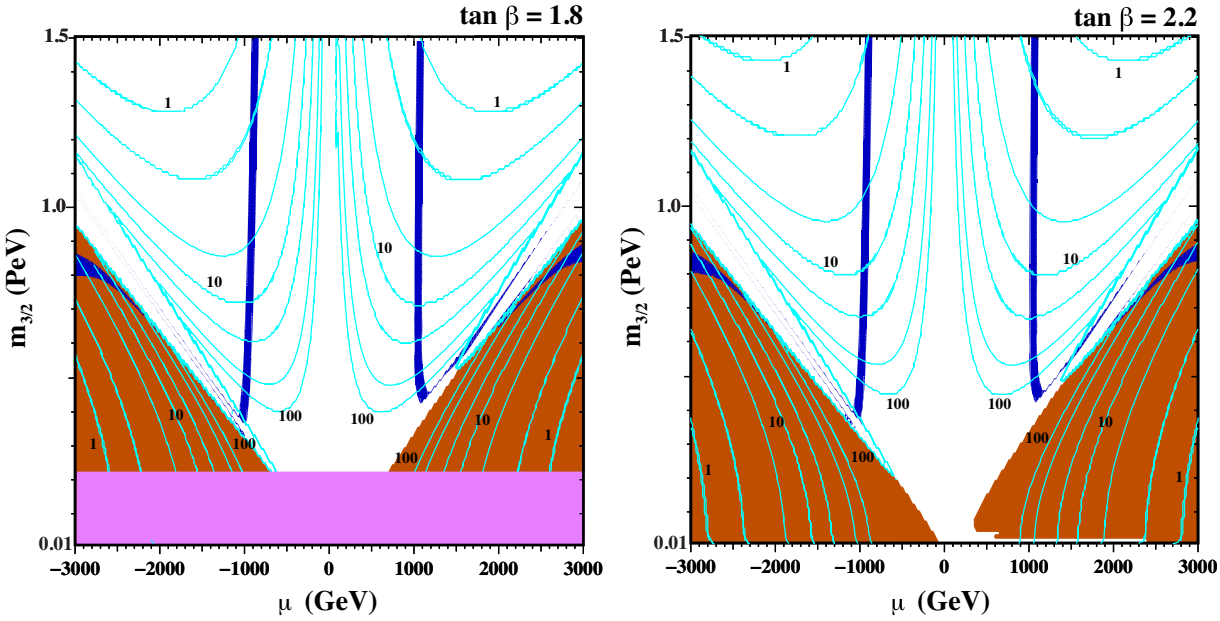

FIG. 7. The spin-dependent elastic cross section for LSP scattering on protons in the $(\mu, m_{3/2})$ plane for fixed $\tan\beta = 1.8$ (left) and 2.2 (right). The shaded regions are the same as in Fig. 2. Values of the cross sections are as labeled in units of 10^{-8} pb. Contours between the labeled decades are 2× and 5× the preceding decade.

which suppress the cross section. The strong dependence on $m_{3/2}$ for low mass occurs as the identity of the LSP changes from wino to Higgsino as $m_{3/2}$ is increased. In addition, the LSP changes between $\tilde{H}_{[1,2]}$ and $\tilde{H}_{(1,2)}$ involving rapid changes in the mixing angles and a strong variation in the cross section. At large values of $m_{3/2}$, the cross section falls beneath the neutrino floor for $\mu < 0$.

Similarly, we plot in Fig. 7 the spin-dependent cross sections, $\sigma_p^{\mathrm{SD}} = \sigma_2$, for $\tan\beta = 1.8$ (left) and 2.2 (right). Cross section values are again as labeled in units of 10^{-8} pb. The current best experimental limit on the spin-dependent cross section comes from PICO [56] and is too weak to be visible on this plane. The strongest constraint 2.5×10^{-5} pb for $m_\chi = 25$ GeV, and is 3.5×10^{-4} for $m_\chi = 1$ TeV. Once again we find a rapid variation in the cross section in the region transitioning between a wino and Higgsino LSP. This is also seen in the one-dimensional plots shown in the left panel of Fig. 8. As one can see, there

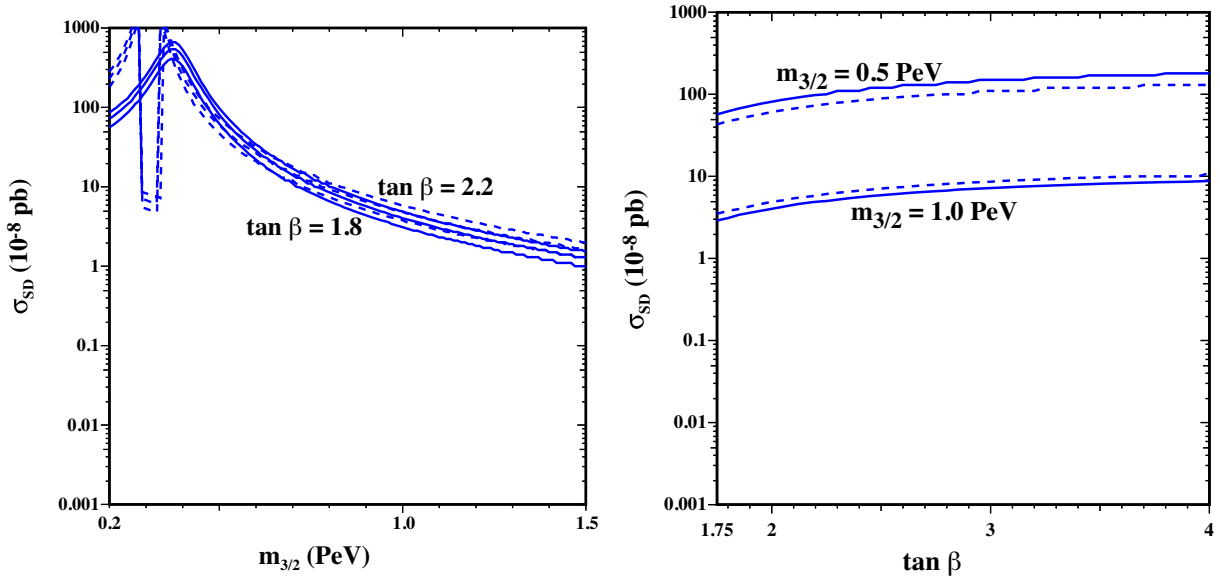

FIG. 8. The spin-dependent elastic cross section for LSP scattering on protons as a function of $m_{3/2}$ (left) for $\tan\beta = 1.8$, 2.0, and 2.2, and as a function of $\tan\beta$ (right) for $m_{3/2} = 0.5$ and 1.0 PeV. In both panels, $\mu = 1080$ GeV (solid) and -900 GeV (dashed).

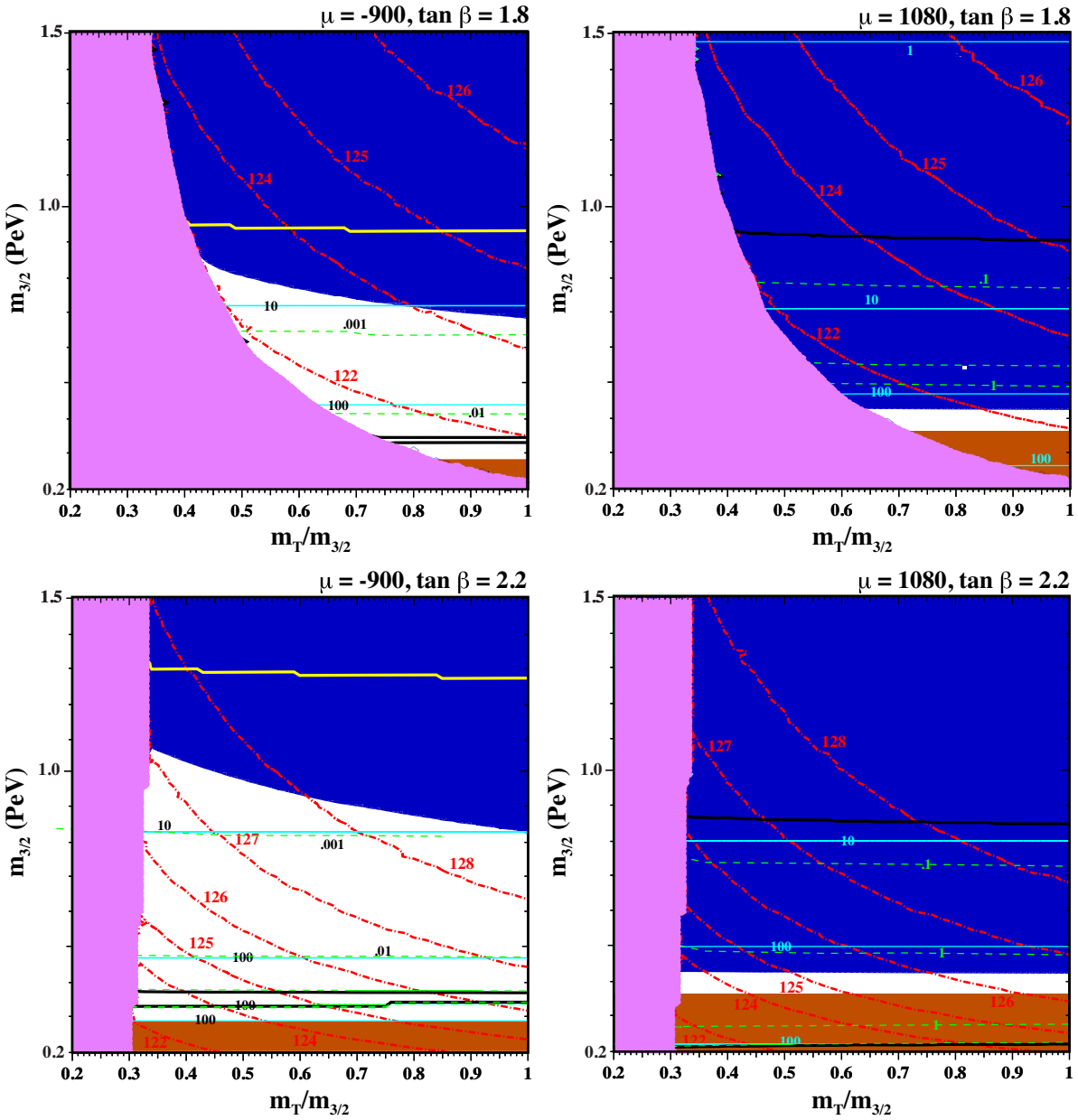

FIG. 9. The $(m_T/m_{3/2}, m_{3/2})$ plane for fixed $\tan\beta = 1.8$ (upper) and 2.2 (lower) for fixed values of $\mu = -900$ GeV (left) and 1080 GeV (right). The pink shaded region is excluded as it contains a tachyonic stop. In the dark red shaded region, there is a wino LSP. In the remainder of the plane, the Higgsino is the LSP. Higgs mass contours, with masses labeled are shown as red dot-dashed curves. Spin-independent cross sections are shown by green dashed lines and spin-dependent cross sections by solid blue lines. For spin-independent cross sections, the experimental upper limit is shown by the solid black line and the neutrino floor by a yellow line.

is far less dependence on the sign of μ for the spin-dependent cross section. This can be readily understood by comparing Eqs. (25) and (26).

Finally, we present in Fig. 9 results in the $(m_T/m_{3/2}, m_{3/2})$ plane where we allow the stop masses to be nonuniversal. More specifically, we set the boundary condition for the third generation left-handed quark doublet and right-handed stop to be m_T at the high energy supersymmetry breaking input scale. We again display results for $\tan\beta = 1.8$ (upper panels) and 2.2 (lower panels) and two fixed values of $\mu = -900$ GeV (left) and 1080 GeV (right). Because we fix μ at a value which leads to $\Omega_\chi h^2 \simeq 0.12$ in the models with universal sfermion masses, large portions of these planes provide the correct relic density as seen by the dark blue shading. For small values of $m_{3/2}$, the LSP is predominantly a wino in the dark red shaded region. For small values of $m_T/m_{3/2}$, one of the stops becomes tachyonic and we shade this region pink. The Higgs masses are shown by red dot-dashed curves as labeled. As one can see in much of the dark blue shaded region with good relic density, the Higgs mass is

similar to the experimental value within uncertainties. Furthermore, for $\tan\beta = 2.2$, more of the parameter space is in agreement with experiment compared to the case of $m_T = m_{3/2}$ as the Higgs mass decreases with $m_T/m_{3/2}$. This means larger values of $\tan\beta$ will have some viable parameter space for $m_T/m_{3/2}$ small. However, it is clear from these figures that $\tan\beta$ can still not be significantly larger than 2.2.

The elastic scattering cross sections are relatively insensitive to the stop masses and are shown in Fig. 9 as nearly horizontal lines. Spin-independent cross sections are shown by green dashed lines and spin-dependent cross sections by solid blue lines labeled in units of 10^{-8} pb. Once again, we see the experimental upper limit (solid black line) and the neutrino floor (yellow line) for $\mu < 0$, applicable for the spin-independent cross section only. Points below the black line are in excess of the experimental bound and points above the yellow line fall beneath the neutrino floor.

V. CONCLUSIONS

Experimental verification of physics beyond the Standard Model is of the utmost importance. We know such physics must be present in order to account for dark matter as well as other aspects of cosmology such as the baryon asymmetry. Supersymmetry is a well studied extension which helps better explain features of the Standard Model as well as providing a dark matter candidate. However because the mechanism for breaking supersymmetry is unknown, there is a very diverse set of supersymmetric models to study. Models such as mSUGRA with weak scale supersymmetry breaking are under considerable pressure, as weak scale superpartners have yet to be discovered [7]. Some high-scale models with an EeV scale gravitino and still higher superpartner masses are extremely challenging from the point of view of discovery [57]. Naively, one might think that models with PeV scalar masses would present similar challenges.

We have considered here PGM models with a PeV gravitino mass (and similarly massive scalars). However, the gaugino masses in these models are loop suppressed and may be of order of ~1 TeV. Further, we have extended the minimal model (with two parameters—$m_{3/2}$ and $\tan\beta$) to include μ as a free parameter, thus easily allowing for the possibility of Higgsino dark matter. Despite the high scalar masses, which allows us to consider the decoupling limit, the dark matter-proton scattering cross sections are *not* unobservably small. We considered the $\mu, m_{3/2}$ parameter space for fixed $\tan\beta$, taking values of $|\mu| \leq 3$ TeV, and $m_{3/2} \leq 1.5$ PeV with $\tan\beta = 1.8$ and 2.2. For higher values of $\tan\beta$, the calculated Higgs mass becomes significantly larger than its measured value (even taking into account theoretical uncertainties in the calculation). To increase the parameter space, we also allowed for the possibility that the stop masses are not universal at the input supersymmetry breaking scale (which we have taken to be the GUT scale). This effect, however, was marginal.

We found that the spin-independent cross section was quite sensitive to the sign of μ. For $\mu > 0$, the current experimental constraint on $\sigma_p^{\rm SI}$ from PandaX-4T [52] excludes gravitino masses below 850 TeV when $\mu \sim 1$ TeV ($m_{3/2} \lesssim 200$ TeV are allowed, as the cross section begins to drop when the LSP is winolike). At larger $m_{3/2}$, the elastic cross sections are large enough to be detected in future experiments. For example, at $m_{3/2} = 1.5$ PeV (with $\mu \sim 1$ TeV), $\sigma_p^{\rm SI} \approx 10^{-10}$ pb well above the neutrino floor at $\approx 2.5 \times 10^{-12}$ pb for $m_\chi \simeq 1$ TeV. In contrast, for $\mu < 0$, the cross section is below the neutrino floor when $m_{3/2} \gtrsim 1$ PeV and is somewhat sensitive to $\tan\beta$ (see Fig. 6). Current experimental results do not place significant bounds on the parameter space when $\mu < 0$. The resulting cross section for spin-dependent interactions remains at least 2 orders of magnitude below current experimental bounds. Nevertheless, we remain hopeful that a signal for Higgsino dark matter in PGM-like models is viable in future direct detection experiments.

ACKNOWLEDGMENTS

J. L. E. would like to thanks Tsutomu T. Yanagida for useful discussions during the early stages of this work. The work of K. A. O. was supported in part by DOE Grant No. DE-SC0011842 at the University of Minnesota.

[1] L. Maiani, Conf. Proc. C **7909031**, 1 (1979); Recent developments in gauge theories, in *Proceedings of the NATO Advanced Study Institute, Cargese, France, 1979*, edited by Gerard 't Hooft *et al.*, NATO Advanced Study Institutes, Ser. B (Plenum Press, New York, 1980), p. 59; Edward Witten, Phys. Lett. **105B**, 267 (1981).
[2] H. Goldberg, Phys. Rev. Lett. **50**, 1419 (1983).
[3] J. Ellis, J. Hagelin, D. Nanopoulos, K. Olive, and M. Srednicki, Nucl. Phys. **B238**, 453 (1984).
[4] John R. Ellis and Douglas Ross, Phys. Lett. B **506**, 331 (2001).
[5] J. R. Ellis, G. Ridolfi, and F. Zwirner, Phys. Lett. B **257**, 83 (1991); **262**, 477 (1991); Y. Okada, M. Yamaguchi, and T. Yanagida, Phys. Lett. B **262**, 54 (1991); Prog. Theor. Phys. **85**, 1 (1991); A. Yamada, Phys. Lett. B **263**, 233 (1991);

Howard E. Haber and Ralf Hempfling, Phys. Rev. Lett. **66**, 1815 (1991); M. Drees and M. M. Nojiri, Phys. Rev. D **45**, 2482 (1992); P. H. Chankowski, S. Pokorski, and J. Rosiek, Phys. Lett. B **274**, 191 (1992); **286**, 307 (1992).

[6] John R. Ellis, S. Kelley, and Dimitri V. Nanopoulos, Phys. Lett. B **249**, 441 (1990); **260**, 131 (1991); Ugo Amaldi, Wim de Boer, and Hermann Furstenau, Phys. Lett. B **260**, 447 (1991); Paul Langacker and Ming-xing Luo, Phys. Rev. D **44**, 817 (1991); C. Giunti, C. W. Kim, and U. W. Lee, Mod. Phys. Lett. A **06**, 1745 (1991).

[7] M. Aaboud *et al.* (ATLAS Collaboration), J. High Energy Phys. 06 (2018) 107; Phys. Rev. D **97**, 112001 (2018); A. M. Sirunyan *et al.* (CMS Collaboration), Eur. Phys. J. C **77**, 710 (2017); J. High Energy Phys. 05 (2018) 025.

[8] T. Moroi, M. Yamaguchi, and T. Yanagida, Phys. Lett. B **342**, 105 (1995); I. Joichi and M. Yamaguchi, Phys. Lett. B **342**, 111 (1995); M. Kawasaki, T. Moroi, and T. Yanagida, Phys. Lett. B **370**, 52 (1996).

[9] J. L. Evans, M. A. G. García, and K. A. Olive, J. Cosmol. Astropart. Phys. 03 (2014) 022.

[10] J. D. Wells, arXiv:hep-ph/0306127; N. Arkani-Hamed and S. Dimopoulos, J. High Energy Phys. 06 (2005) 073; G. F. Giudice and A. Romanino, Nucl. Phys. **B699**, 65 (2004); **B706**, 65(E) (2005); N. Arkani-Hamed, S. Dimopoulos, G. F. Giudice, and A. Romanino, Nucl. Phys. **B709**, 3 (2005); J. D. Wells, Phys. Rev. D **71**, 015013 (2005).

[11] M. Ibe, T. Moroi, and T. T. Yanagida, Phys. Lett. B **644**, 355 (2007); M. Ibe and T. T. Yanagida, Phys. Lett. B **709**, 374 (2012); M. Ibe, S. Matsumoto, and T. T. Yanagida, Phys. Rev. D **85**, 095011 (2012).

[12] B. Bhattacherjee, B. Feldstein, M. Ibe, S. Matsumoto, and T. T. Yanagida, Phys. Rev. D **87**, 015028 (2013).

[13] N. Arkani-Hamed, A. Gupta, D. E. Kaplan, N. Weiner, and T. Zorawski, arXiv:1212.6971.

[14] J. L. Evans, M. Ibe, K. A. Olive, and T. T. Yanagida, Eur. Phys. J. C **73**, 2468 (2013).

[15] J. L. Evans, K. A. Olive, M. Ibe, and T. T. Yanagida, Eur. Phys. J. C **73**, 2611 (2013).

[16] K. Harigaya, M. Ibe, and T. T. Yanagida, J. High Energy Phys. 12 (2013) 016; J. L. Evans and K. A. Olive, arXiv:1408.5102.

[17] J. L. Evans, M. Ibe, K. A. Olive, and T. T. Yanagida, Phys. Rev. D **91**, 055008 (2015).

[18] J. L. Evans, N. Nagata, and K. A. Olive, Phys. Rev. D **91**, 055027 (2015).

[19] M. Dine and D. MacIntire, Phys. Rev. D **46**, 2594 (1992); L. Randall and R. Sundrum, Nucl. Phys. **B557**, 79 (1999); G. F. Giudice, M. A. Luty, H. Murayama, and R. Rattazzi, J. High Energy Phys. 12 (1998) 027; J. A. Bagger, T. Moroi, and E. Poppitz, J. High Energy Phys. 04 (2000) 009; P. Binetruy, M. K. Gaillard, and B. D. Nelson, Nucl. Phys. **B604**, 32 (2001).

[20] L. E. Ibanez and G. G. Ross, Phys. Lett. B **110**, 215 (1982); K. Inoue, A. Kakuto, H. Komatsu, and S. Takeshita, Prog. Theor. Phys. **68**, 927 (1982); **70**, 330(E) (1983); **70**, 330 (1983); L. E. Ibanez, Phys. Lett. **118B**, 73 (1982); J. R. Ellis, D. V. Nanopoulos, and K. Tamvakis, Phys. Lett. **121B**, 123 (1983); J. R. Ellis, J. S. Hagelin, D. V. Nanopoulos, and K. Tamvakis, Phys. Lett. **125B**, 275 (1983); L. Alvarez-Gaume, J. Polchinski, and M. B. Wise, Nucl. Phys. **B221**, 495 (1983).

[21] R. Barbieri, S. Ferrara, and C. A. Savoy, Phys. Lett. **119B**, 343 (1982).

[22] J. R. Ellis, K. A. Olive, Y. Santoso, and V. C. Spanos, Phys. Lett. B **573**, 162 (2003); Phys. Rev. D **70**, 055005 (2004).

[23] G. F. Giudice and A. Masiero, Phys. Lett. B **206**, 480 (1988).

[24] K. Inoue, M. Kawasaki, M. Yamaguchi, and T. Yanagida, Phys. Rev. D **45**, 328 (1992).

[25] E. Dudas, Y. Mambrini, A. Mustafayev, and K. A. Olive, Eur. Phys. J. C **72**, 2138 (2012).

[26] J. Hisano, S. Matsumoto, M. Nagai, O. Saito, and M. Senami, Phys. Lett. B **646**, 34 (2007).

[27] M. Cirelli, A. Strumia, and M. Tamburini, Nucl. Phys. **B787**, 152 (2007); A. Hryczuk, R. Iengo, and P. Ullio, J. High Energy Phys. 03 (2011) 069; M. Beneke, A. Bharucha, F. Dighera, C. Hellmann, A. Hryczuk, S. Recksiegel, and P. Ruiz-Femenia, J. High Energy Phys. 03 (2016) 119.

[28] E. Bagnaschi, M. Borsato, K. Sakurai, O. Buchmueller, R. Cavanaugh, V. Chobanova, M. Citron, J. C. Costa, A. De Roeck, M. J. Dolan *et al.*, Eur. Phys. J. C **77**, 268 (2017).

[29] A. Sommerfeld, Ann. Phys. (N.Y.) **403**, 257 (1931).

[30] N. Aghanim *et al.* (Planck Collaboration), Astron. Astrophys. **641**, A6 (2020); **652**, C4 (2021).

[31] T. Cohen, M. Lisanti, A. Pierce, and T. R. Slatyer, J. Cosmol. Astropart. Phys. 10 (2013) 061.

[32] J. Fan and M. Reece, J. High Energy Phys. 10 (2013) 124.

[33] M. Baumgart, I. Z. Rothstein, and V. Vaidya, J. High Energy Phys. 04 (2015) 106.

[34] H. Baer, A. Mustafayev, S. Profumo, A. Belyaev, and X. Tata, Phys. Rev. D **71**, 095008 (2005); H. Baer, A. Mustafayev, S. Profumo, A. Belyaev, and X. Tata, J. High Energy Phys. 07 (2005) 065; J. R. Ellis, K. A. Olive, and P. Sandick, Phys. Rev. D **78**, 075012 (2008).

[35] J. Ellis, K. Olive, and Y. Santoso, Phys. Lett. B **539**, 107 (2002); J. R. Ellis, T. Falk, K. A. Olive, and Y. Santoso, Nucl. Phys. **B652**, 259 (2003).

[36] K. A. Olive and M. Srednicki, Phys. Lett. B **230**, 78 (1989); Nucl. Phys. **B355**, 208 (1991).

[37] A. Delgado and M. Quirós, Phys. Rev. D **103**, 015024 (2021); K. Kowalska and E. M. Sessolo, Adv. High Energy Phys. **2018**, 6828560 (2018).

[38] B. Dutta and Y. Mimura, Phys. Lett. B **627**, 145 (2005).

[39] N. Nagata and S. Shirai, J. High Energy Phys. 01 (2015) 029.

[40] V. Suryanarayana Mummidi and K. M. Patel, Phys. Rev. D **101**, 115008 (2020).

[41] R. T. Co, B. Sheff, and J. D. Wells, Phys. Rev. D **105**, 035012 (2022).

[42] J. R. Ellis and D. V. Nanopoulos, Phys. Lett. B **110**, 44 (1982).

[43] J. L. Feng, K. T. Matchev, and T. Moroi, Phys. Rev. Lett. **84**, 2322 (2000); H. Baer, T. Krupovnickas, S. Profumo, and P. Ullio, J. High Energy Phys. 10 (2005) 020; J. L. Feng, K. T. Matchev, and D. Sanford, Phys. Rev. D **85**, 075007 (2012); P. Draper, J. Feng, P. Kant, S. Profumo, and D. Sanford, Phys. Rev. D **88**, 015025 (2013).

[44] M. Dine, R. Kitano, A. Morisse, and Y. Shirman, Phys. Rev. D **73**, 123518 (2006); R. Kitano, Phys. Lett. B **641**, 203 (2006); E. Dudas, C. Papineau, and S. Pokorski, J. High

Energy Phys. 02 (2007) 028; H. Abe, T. Higaki, T. Kobayashi, and Y. Omura, Phys. Rev. D **75**, 025019 (2007); R. Kallosh and A. D. Linde, J. High Energy Phys. 02 (2007) 002; H. Abe, T. Higaki, and T. Kobayashi, Phys. Rev. D **76**, 105003 (2007); J. Fan, M. Reece, and L.-T. Wang, J. High Energy Phys. 09 (2011) 126; Y. Ema, R. Kitano, and T. Terada, J. High Energy Phys. 09 (2018) 075.

[45] E. Dudas, A. Linde, Y. Mambrini, A. Mustafayev, and K. A. Olive, Eur. Phys. J. C **73**, 2268 (2013); M. Bose, M. Dine, and P. Draper, Phys. Rev. D **88**, 023533 (2013); M. A. G. García and K. A. Olive, J. Cosmol. Astropart. Phys. 09 (2013) 007.

[46] V. D. Barger, M. S. Berger, and P. Ohmann, Phys. Rev. D **49**, 4908 (1994); W. de Boer, R. Ehret, and D. I. Kazakov, Z. Phys. C **67**, 647 (1995); M. Carena, J. R. Ellis, A. Pilaftsis, and C. E. Wagner, Nucl. Phys. **B625**, 345 (2002).

[47] J. Ellis and R. Flores, Nucl. Phys. **B307**, 883 (1988); Phys. Lett. B **263**, 259 (1991); **300**, 175 (1993); R. Flores, K. A. Olive, and M. Srednicki, Phys. Lett. B **237**, 72 (1990).

[48] K. Griest, Phys. Rev. D **38**, 2357 (1988); R. Barbieri, M. Frigeni, and G. Giudice, Nucl. Phys. **B313**, 725 (1989); R. Flores, K. A. Olive, and M. Srednicki, Phys. Lett. B **237**, 72 (1990); M. Drees and M. M. Nojiri, Phys. Rev. D **48**, 3483 (1993); V. Bednyakov, H. V. Klapdor-Kleingrothaus, and S. Kovalenko, Phys. Rev. D **50**, 7128 (1994); H. Baer and M. Brhlik, Phys. Rev. D **57**, 567 (1998); U. Chattopadhyay, T. Ibrahim, and P. Nath, Phys. Rev. D **60**, 063505 (1999).

[49] T. Falk, A. Ferstl, and K. A. Olive, Phys. Rev. D **59**, 055009 (1999); **60**, 119904(E) (1999); Astropart. Phys. **13**, 301 (2000); J. R. Ellis, A. Ferstl, and K. A. Olive, Phys. Lett. B **481**, 304 (2000); **532**, 318 (2002); J. R. Ellis, A. Ferstl, K. A. Olive, and Y. Santoso, Phys. Rev. D **67**, 123502 (2003).

[50] J. Ellis, N. Nagata, and K. A. Olive, Eur. Phys. J. C **78**, 569 (2018).

[51] J. Billard, L. Strigari, and E. Figueroa-Feliciano, Phys. Rev. D **89**, 023524 (2014); P. Cushman, C. Galbiati, D. N. McKinsey, H. Robertson, T. M. P. Tait, D. Bauer, A. Borgland, B. Cabrera *et al.*, arXiv:1310.8327.

[52] Y. Meng *et al.* (PandaX-4T Collaboration), Phys. Rev. Lett. **127**, 261802 (2021).

[53] R. L. Arnowitt, B. Dutta, and Y. Santoso, Nucl. Phys. **B606**, 59 (2001).

[54] H. Baer, C. Balazs, A. Belyaev, and J. O'Farrill, J. Cosmol. Astropart. Phys. 09 (2003) 007.

[55] C. Cheung, L. J. Hall, D. Pinner, and J. T. Ruderman, J. High Energy Phys. 05 (2013) 100; P. Huang and C. E. M. Wagner, Phys. Rev. D **90**, 015018 (2014); T. Han, F. Kling, S. Su, and Y. Wu, J. High Energy Phys. 02 (2017) 057.

[56] C. Amole *et al.* (PICO Collaboration), Phys. Rev. D **100**, 022001 (2019).

[57] E. Dudas, Y. Mambrini, and K. Olive, Phys. Rev. Lett. **119**, 051801 (2017); E. Dudas, T. Gherghetta, K. Kaneta, Y. Mambrini, and K. A. Olive, Phys. Rev. D **98**, 015030 (2018).